Luminescence-Based Temperature Mapping at Turbine Engine Temperatures Using Breakthrough Cr-Doped $GdAlO_3$ Broadband Luminescence

Project WBS Number: 694478.02.93.02.11.15.22

Investigator(s): Jeffrey Eldridge (RHI), Tim Bencic (RHI), and Dongming Zhu (RXD)

Purpose

The objective of this project is to develop a temperature-sensing capability well suited to making temperature measurements in a turbine engine environment, based on a recent NASA-developed breakthrough temperature-sensing phosphor, Cr-doped $GdAlO_3$. Prior to the NASA discovery of this new temperature-sensing phosphor that exhibits unprecedented intensity at high temperatures, luminescence-based temperature sensing produced inadequate signal strength in the presence of a strong radiative background such as is present in turbine engine environments. The Cr-doped $GdAlO_3$ phosphor overcomes this limitation and will provide key advantages over the currently employed turbine engine temperature measurement technologies.

Background

Presently, thermocouples and pyrometry are the technologies utilized for turbine engine temperature measurements, but both have serious disadvantages for application in a turbine environment. Thermocouples require sensor attachment and only acquire spot measurements, while pyrometry suffers from issues of unknown surface emissivity and interference from reflected radiation. Luminescence-based temperature sensing can overcome these limitations and can be developed to provide 2D temperature mapping of surfaces and to provide robust temperature measurements that are insensitive to radiative backgrounds. The salient characteristic of the Cr-doped $GdAlO_3$ phosphor that will make these measurements possible at turbine engine temperatures is the exceptionally high strength crystal field at the Cr^{3+} dopant site in the perovskite crystal structure, which results in a high energy barrier for non-radiative relaxation. This energy barrier suppresses thermal quenching until much higher temperatures than in phosphors used in the past.

Transition metal dopants such as Cr are not normally considered for thermographic-phosphor-based temperature measurements above 1000ºC due to the aforementioned thermal quenching at lower temperatures. In addition, spin-allowed broadband luminescence emission by transition metal dopants is not usually suitable for thermographic phosphor measurements due to the extremely short radiative decay times and stronger thermal quenching than the spin-forbidden R-line emission. However, Zhang et al. (Zhang, Z., Grattan, K.T.V., and Palmer, A.W., *Phys. Rev. B* **48**, 7772-7778 (1993)) have shown that in high-crystal-field Cr^{3+}-doped crystals, the long-lived ^2E energy level can act as a reservoir for the higher lying $^4T_2$ energy level that is responsible for the spin-allowed broadband emission via radiative relaxation to the $^4A_2$ ground state. Fig. 1 shows a single configurational coordinate diagram for high-crystal-field (where the $^4T_2$ level is higher in energy than the ^2E level) Cr^{3+}-doped crystals such as $Cr:Al_2O_3$ and $Cr:GdAlO_3$, where ΔE is the energy difference between the $^4T_2$ and underlying 2E levels, ΔEq is the energy barrier between the zero-phonon $^4T_2$ state to the $^4T_2$–to-$^4A_2$ crossover by multiphonon absorption, and Δ_{FC} is the Franck-Condon offset between the $^4T_2$ and $^4A_2$ parabolas. At increasing temperatures, thermal equilibrium between the ^2E and $^4T_2$ levels results in an increasing promotion of ions from the much longer-lived ^2E reservoir level to the $^4T_2$ level. Therefore, the spin-allowed broadband radiative relaxation from the $^4T_2$ to $^4A_2$ ground state increases as the emission associated with the spin-forbidden ^2E to $^4A_2$ radiative transition decreases. At even higher temperatures, non-radiative crossover from the $^4T_2$ to $^4A_2$ states increases due to higher phonon population levels

and leads to the eventual thermal quenching of the spin-allowed broadband emission. Because thermal equilibrium is maintained between the ^2E and $^4T_2$ populations, the observed decay time of the observed ^2E to $^4A_2$ emission, τ_{2E}, and that of the $^4T_2$ to $^4A_2$ broadband emission, τ_{4T2}, both reflect the depopulation of the ^2E reservoir. Therefore, $\tau_{2E} = \tau_{4T2}$. Zhang et al. showed that the decay time associated with these ^2E reservoir depopulation processes as a function of temperature, T, can be expressed by:

$$\tau_{4T2} = \tau_{2E} = \tau_{2E}^{R} \frac{1+3e^{-\Delta E/kT}}{1+\alpha e^{-\Delta E/kT}+\beta e^{-(\Delta Eq+\Delta E)/kT}} \quad (1)$$

where $1/\tau_{2E}^{R}$ is the intrinsic radiative rate of the ^2E to $^4A_2$ transition, $\alpha = \tau_{2E}^{R}/\tau_{4T2}^{R}$, $\beta = \tau_{2E}^{R}/\tau_q$, $1/\tau_{4T2}^{R}$ is the intrinsic radiative rate of the $^4T_2$ to $^4A_2$ transition, $1/\tau_q$ is a scaling factor for the nonradiative $^4T_2$ to $^4A_2$ crossover rate, and k is Boltzmann's constant. Assuming α and $\beta \gg 1$, this relationship shows that thermal quenching of the observed broadband $^4T_2$ to $^4A_2$ transition can be delayed to higher temperatures by increases in ΔE and in ΔEq. The Tanabe-Sugano diagram for $3d^3$ electron configurations (Fig. 2) indicates that ΔE increases with the strength of the crystal field. Furthermore, ΔEq becomes greater for stronger bonding, since the stronger restoring force on a displaced ion will result in a greater steepening of the $^4T_2$ parabola (involves bonding orbitals) than the $^4A_2$ parabola (does not involve bonding orbitals).

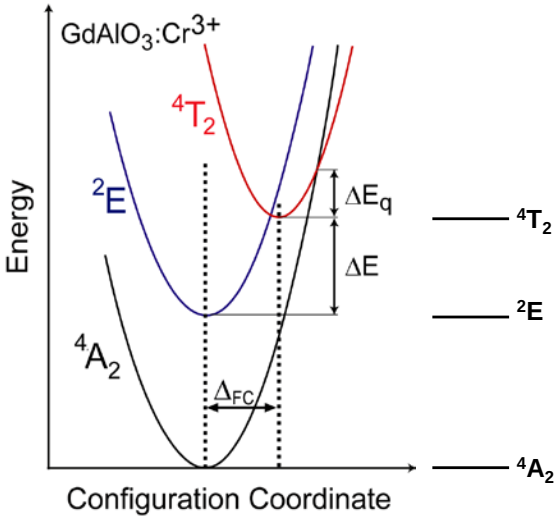

Figure 1. Single configurational coordinate plot (left) and energy level diagram (right) for high-crystal-field Cr^{3+}-doped phosphors such as Cr:$GdAlO_3$.

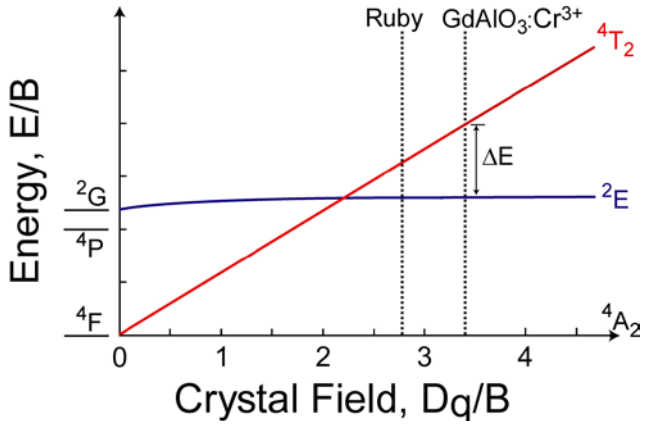

Figure 2. Tanabe-Sugano diagram showing relationship between $^4T_2$ and ^2E energy levels and crystal field for Cr^{3+} $3d^3$ electron configuration. Dotted lines show that higher crystal field in Cr:$GdAlO_3$ will lead to substantially higher energy difference between these levels compared to ruby.

In view of these considerations, rare-earth aluminate orthorhombic perovskites, $REAlO_3$, are ideal crystal hosts for Cr^{3+} dopants. The Cr^{3+} dopant ions substitute for the Al^{3+} ions in the tightly bound AlO_6 octahedra within the $REAlO_3$ perovskite structure, resulting in exceptionally strong crystal fields (20% higher at Al^{3+} sites in $GdAlO_3$ compared to Al_2O_3) and therefore a substantially greater ΔE as shown in Fig. 2. Among the rare-earth aluminate perovskites, $REAlO_3$, only the perovskites with RE = Gd, Tb, Dy, Y, Ho, Er, and Tm retain an orthorhombic perovskite structure from room temperature to above 1000ºC. The others exist in either rhombohedral or cubic structures, with undistorted cubic symmetry at the Al^{3+} sites in the AlO_6 octahedra, and therefore will exhibit undesirably weak excitation transition oscillator strengths. Among the remaining candidate rare-earths, the crystal field at the Al^{3+} octahedral sites is expected to decrease in the order from largest to smallest ionic radii (Gd>Tb>Dy>Y>Ho>Er>Tm). Therefore, Cr:$GdAlO_3$ is expected to delay thermal quenching of the spin-allowed broadband emission to higher temperatures than the other perovskite candidates.

The development of this approach for acquiring accurate non-contact temperature

measurements in a turbine engine environment is an important objective for ARMD for overcoming the unsuitability of thermocouples and pyrometry for making turbine engine temperature measurements. This new capability will enable NASA to validate the influence of engine operating temperatures on clean fuel burn and to evaluate the effectiveness of cooling strategies for turbine component surfaces.

Approach

The innovative luminescence-based temperature measurement concept **was** adapted in two implementations: (1) development of an optical thermometer for probing combustion gas temperatures and (2) 2D temperature mapping of component surfaces. For the optical thermometer demonstration, small diameter sapphire and quartz rods and fibers are end-coated with a Cr-doped $GdAlO_3$ layer that can then be inserted into a furnace environment to evaluate both the temperature measurement range and sensitivity.
For the 2D temperature mapping, cooling holes were laser-drilled into thermal barrier coated specimens. The specimens are then coated with a thin layer of the Cr-doped $GdAlO_3$ phosphor. These specimens will be exposed to high heat flux laser heating while cooling air is forced through the cooling holes from the specimen backside. Time-gated imaging techniques synchronized with laser excitation will then be used for producing 2D surface maps of the temperature gradients around the cooling holes.

Summary of Research

Demonstration of Temperature Measurement Capability

The first stage of the project involved producing specimens for testing and temperature calibration and assembling optical test instrumentation to perform the desired measurements. Specimens were 1” diameter pucks produced by sintering Cr:$GdAlO_3$ powder with a 0.2% Cr^{3+} cation doping level. The puck was placed inside a box furnace with two access holes in the back. Excitation by a pulsed 20 Hz, 532 nm (frequency double YAG:Nd) laser was transmitted through one of the access holes while luminescence emission was collected by a collection optics assembly with a 125 mm working distance through the other access hole. Fig. 3 shows an excitation spectrum obtained from a Cr:$GdAlO_3$ specimen, showing the choice of the 532 nm excitation was made from a very wide range of excitation wavelengths that could be selected. As a basis for selecting a wavelength range for collection of luminescence, luminescence emission spectra (Fig. 4) were acquired using an existing optical set-up as a function of temperature from Cr:GAP specimens under pulsed laser excitation. These spectra showed the growth of the desired broadband emission centered at 640 nm as well as the decrease in the better-known R-line emission at 728 nm and the Stokes phonon-loss peak at 700 nm with increasing temperature. It also became apparent that at the highest temperatures, the shorter-wavelength broadband emission dominates the emission spectrum and therefore is the only component of luminescence emission that can be utilized for turbine engine temperature measurements.

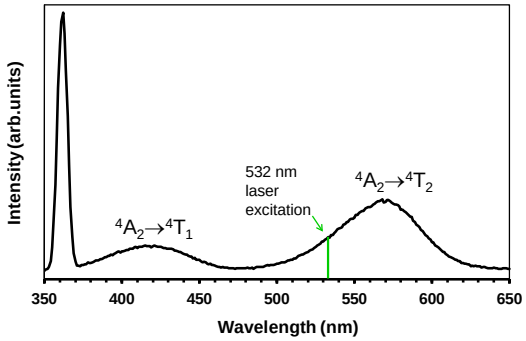

Figure 3. Room temperature excitation spectrum for Cr:$GdAlO_3$. Emission at 728 nm.

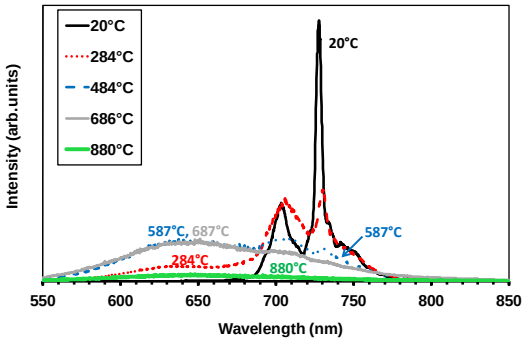

Figure 4. Temperature dependence of luminescence emission spectra for Cr:GAP. Excitation at 532 nm.

Since temperature measurements were to be based on luminescence decay measurements, the decay behavior of the luminescence emission spectra was evaluated as a function of temperature. For this purpose, a time-resolved luminescence emission set-up (Fig. 5) was assembled, where a pulsed 532 nm laser was aimed through a hole in the furnace where the Cr:GAP puck was positioned. The luminescence emission was then collected using a 1" diameter optics assembly and that light was then routed to a spectrograph where the dispersed light was collected by a gated ICCD for time-resolved spectra. Time-resolved luminescence emission spectra at 15ºC and 1072ºC are shown in Figs. 6-7. Fig. 6a shows the decay of the sharp R-line emission and vibrational side bands at 15ºC. The same data is rearranged from the series of spectra collected at different delay times to a series of decay measurements at different wavelengths and then replotted in Fig. 6b with a logarithmic intensity scale. The uniform downward slope across the full range of luminescence emission in Fig. 6b reveals a uniform exponential decay (with decay time τ = 13.1 msec) across this range. Fig. 7a displays the time-resolved spectra acquired at 1072ºC, with only broadband emission remaining at this temperature. Fig. 7b, replotted as a series of decay curves at different wavelengths on a logarithmic intensity scale, shows a uniform luminescence decay rate (with τ = 1.5 µsec) for the broadband luminescence emission at 1072ºC. The significance of this finding for temperature measurements is that the same decay-time/temperature calibration will be maintained for any choice of wavelength range. Therefore, the wavelength range selection can be based purely on consideration of signal intensity and avoidance of competing thermal radiation background.

Fig. 7b shows that while the peak emission intensity is at 660 nm, there is still more than adequate signal intensity at 570 nm to accurately determine a luminescence decay constant. Because the blackbody thermal radiation background in a turbine engine environment is much lower at the shorter wavelengths, it was decided that the optical thermometer and 2D temperature measurements would be based on using a bandpass filter that selects a luminescence emission wavelength range centered at 590 nm with a full-width half-max of 40 nm. The wavelength range collected using this bandpass filter is shown shaded in red in Fig. 7b.

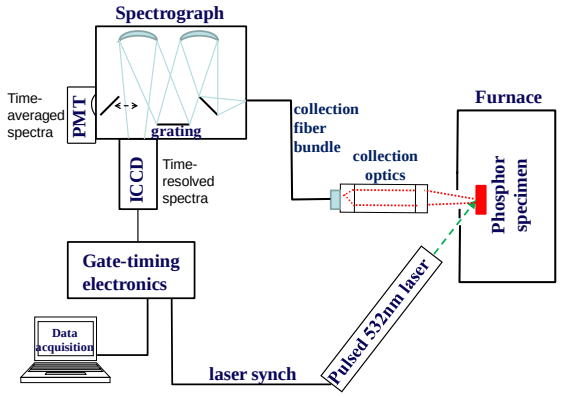

Figure 5. Time-resolved luminescence emission set-up.

Luminescence decay curves acquired at various temperatures up to 1076ºC using this bandpass filter are shown in Fig. 8. Although these decay curves are nearly single exponential, they were fitted by a double exponential equation to account for the short, fast initial decay: $I = I_1 e^{-t/\tau_1} + I_2 e^{-t/\tau_2}$, where I is the intensity, t is time, τ_1 is the time constant associated with the short initial decay, and τ_2 is the time constant associated with the dominant long-term decay. The values of τ_2 were used for temperature calibration.

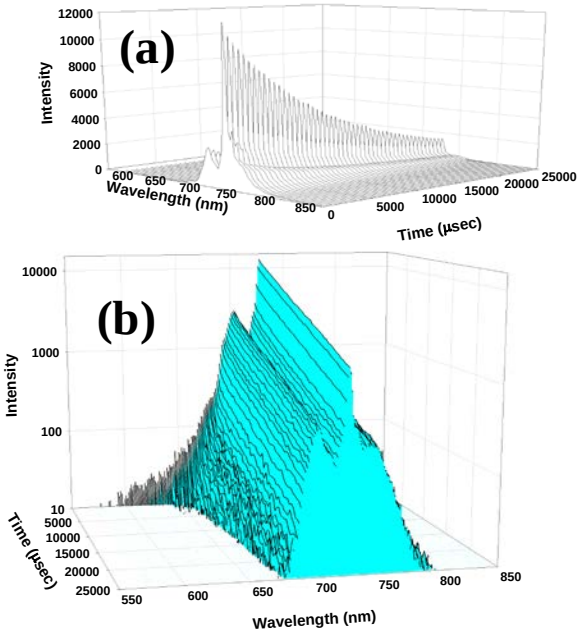

Figure 6. 3D plots showing time-resolved decay of luminescence emission spectra from Cr:GAP at 15ºC. (a) Linear intensity scale. (b) Logarithmic intensity scale shows uniform slope over full wavelength range, indicating wavelength-independent decay time.

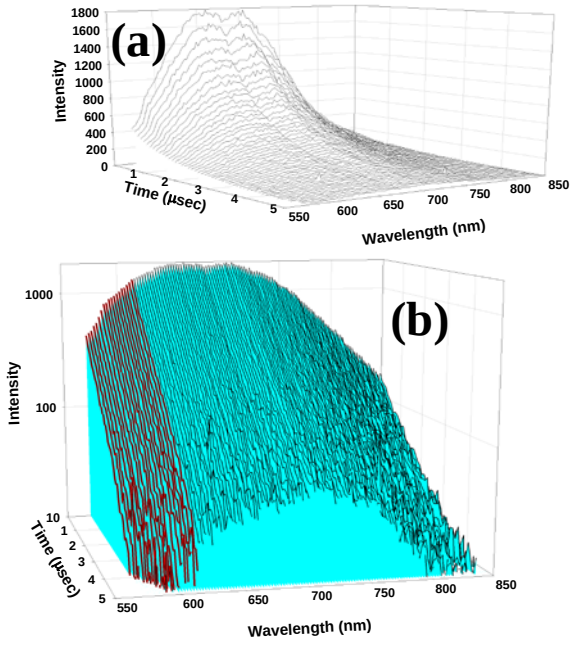

Figure 7. 3D plots showing time-resolved decay of luminescence emission spectra from Cr:GAP at 1072ºC. (a) Linear intensity scale. (b) Logarithmic intensity scale shows uniform slope over full wavelength range, indicating wavelength-independent decay time. Wavelength range shaded in red selected for collection through bandpass filter.

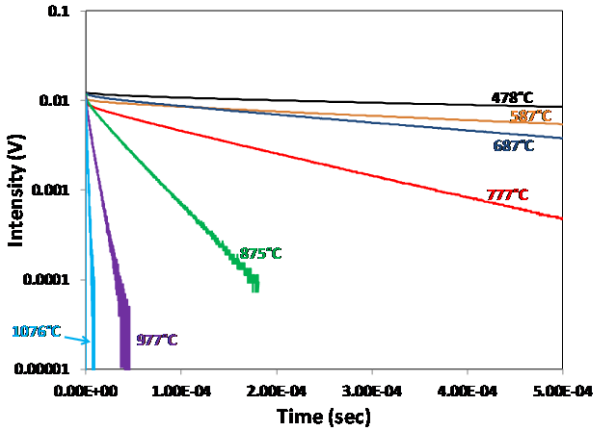

Figure 8. Luminescence decay at various temperatures from Cr:GAP. Using bandpass filter centered at 590 nm with a full-width half-max of 40 nm.

Based on the determined decay constants, a calibration between decay time and temperature up to 1076ºC (the furnace limit) is shown in Fig. 9. Equation 1, which describes the temperature dependence of the broadband emission decay with an underlying reservoir energy level, was fitted to decay time vs. temperature data. The solid black line in Fig. 9 is the fit of this model to the data. Both the data and model show two distinct regimes of luminescence decay: a less temperature sensitive region between about 200ºC and 750ºC and a more temperature sensitive region at temperatures above 750ºC.

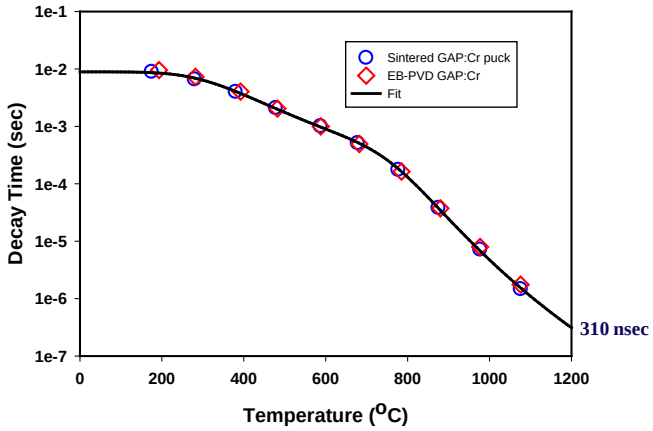

Figure 9. Temperature dependence of Cr:GAP luminescence decay time for wavelengths selected by bandpass filter centered at 590 nm with a full-width half-max of 40 nm. Circles are values determined from measurements of Cr:GAP puck. Diamonds are values from measurements of EB-PVD Cr:GAP coating. Solid line is obtained by fitting the model of Zhang, Grattan, and Palmer to the data.

Optical Thermometer

Based on the investigation of the luminescence decay behavior described above, prototype optical thermometers were constructed out of a set of quartz and sapphire rods with a Cr:GAP layer applied to the rod tips using a "paint" consisting of the phosphor powder suspended in a commercial binder solution followed by heat treatment. Fig. 10 (top) illustrates the experimental arrangement where the optical thermometer consists of a quartz or sapphire lightpipe with a Cr:GAP coating on its tip. In this configuration, both the excitation and emission share the same optical path within the sapphire probe. Fig. 10 (bottom) shows an operating quartz-rod-based optical thermometer with its temperature-sensing end inserted into the back of a furnace.

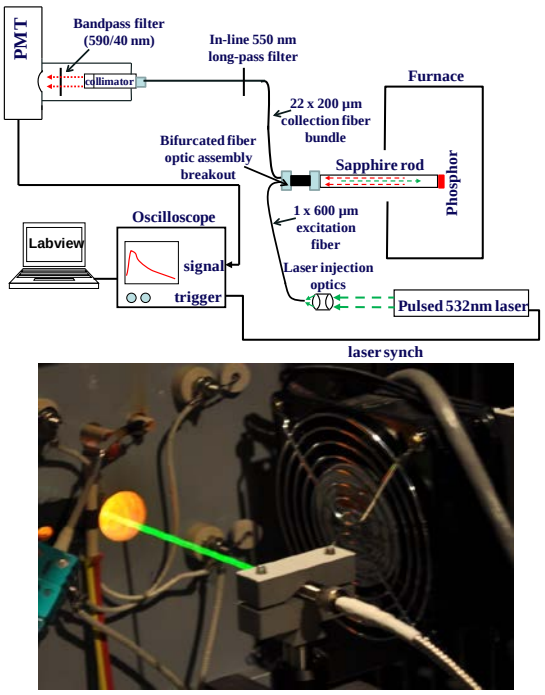

Figure 10. (Top) Schematic of optical thermometer setup. (Bottom) Green laser excitation visible inside of optical thermometer, consisting of quartz rod end-coated with Cr:GAP. Thermometer inserted into furnace.

The quartz rod optical thermometers gave excellent results at lower temperatures, as shown at 680ºC in Fig. 11a. The luminescence decay rate observed for the optical thermometer (red) agrees well with the decay observed for the phosphor alone (black), except at short times where the optical thermometer response exhibits a convolution of the phosphor (black) and phosphor-free quartz rod (blue) responses. Fortunately, the phosphor response is easily decoupled from the phosphor-free quartz rod response at 680ºC. However, Fig. 11b shows that at 875ºC the phosphor decay rate (black) is intermediate between the fast and slow decay components of the quartz rod, so that it difficult to extract the phosphor response from the optical thermometer response (red). It was concluded that the quartz rods and fibers produced usable decay curves up to about 800ºC, above which the intrinsic luminescence from the quartz lightpipe itself interfered with the luminescence from the Cr:GAP at the probe tip.

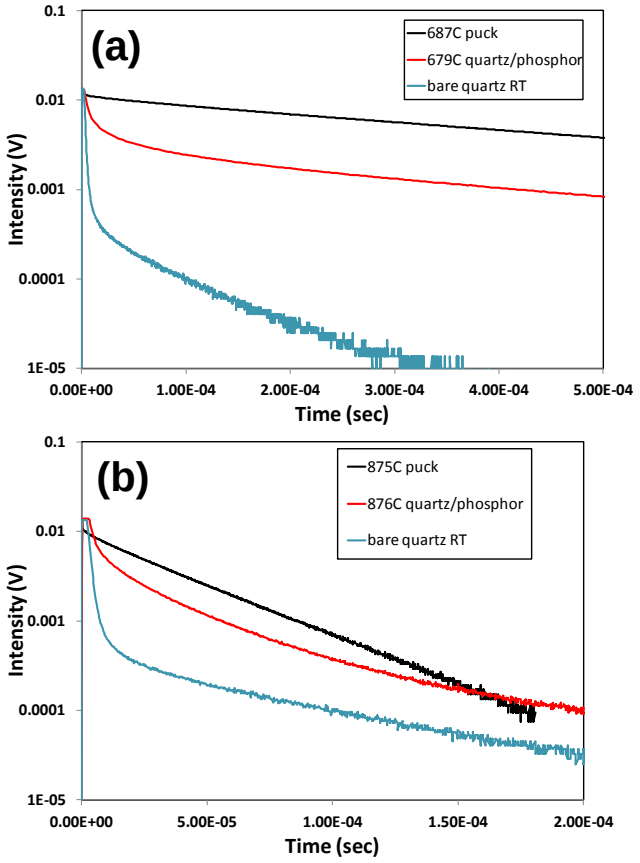

Figure 11. Comparison of luminescence decay for freestanding Cr-doped $GdAlO_3$ puck, Cr-doped $GdAlO_3$ at tip of quartz rod optical thermometer, and bare quartz rod. (a) 680ºC. (b) 875ºC.

Superior results were obtained from a 2 mm diameter sapphire rod. Fig. 12 shows good agreement between the decay curves obtained from the sapphire rod optical thermometer with decay from the Cr:GAP puck up to 1076ºC. Fig.

12 also shows that the bare sapphire rod shows some luminescence from Cr impurities (green curve). This long decay time component is observed in the optical thermometer decays as a modest upward deviation from linearity at long decay times, which is easily corrected for. To produce less-intrusive temperature probes, optical thermometers were also constructed from 400 µm diameter sapphire fibers produced by edge defined growth (EDG), but Fig. 13 shows that the luminescence from the bare fiber was much stronger than in the rods and overwhelmed the luminescence from the Cr:GAP tip, presumably due to significantly higher Cr impurities in the sapphire fibers. In contrast to the sapphire rods, the strong luminescence from Cr^{3+} impurities in the fibers prevents these fibers from performing as effective lightpipes in an optical thermometer. This issue is being addressed by two alternate routes: (1) procuring sapphire fibers manufactured by laser pedestal growth (LPG), which is known to introduce less metallic impurities than the fibers produced by EFG and therefore should contain lower Cr impurities levels and (2) procuring YAG fibers, because Cr impurities in YAG produce much less intense luminescence than in sapphire. Both the higher purity sapphire fibers and the YAG fibers have been received, and confirmation of accurate fiber-based optical thermometer measurements is waiting for a laser repair that should be completed in August 2012.

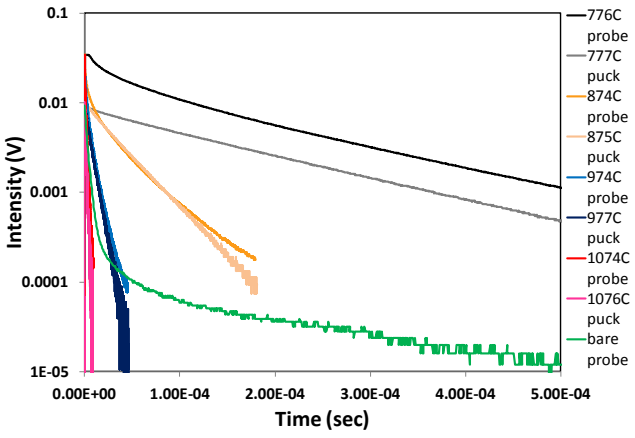

Figure 12. Luminescence decay at various temperatures from Cr:GAP on tip of 2 mm diameter sapphire optical thermometer vs. decay from Cr:GAP puck. Green curve shows decay from bare sapphire rod.

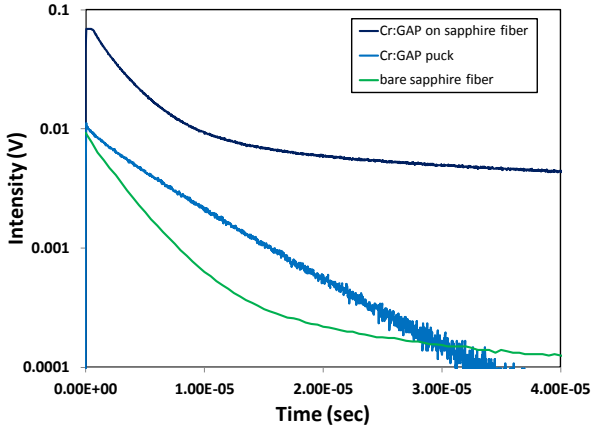

Figure 13. Luminescence decay at 975ºC from Cr:GAP on tip of 400 µm diameter EFG sapphire fiber optical thermometer vs. decay from Cr:GAP puck. Green curve shows decay from bare sapphire fiber. Note similar shape decay curves for Cr:GAP on sapphire fiber and bare sapphire fiber, indicating intrinsic fiber luminescence overwhelms luminescence from Cr:GAP at tip.

Coatings for 2D Temperature Mapping

The 2D temperature mapping around cooling holes to proceeded more slowly than the optical thermometer development due to the series of long-lead-time steps that had to be followed in series rather than in parallel. First, ingots of the phosphor material were fabricated for electron-beam vapor deposition (EB-PVD). TBC-coated 1” button specimens were produced with arrays of 0.020” diameter cooling holes. Samples were produced with cooling holes either 90º (straight through) or 20º (glancing) angles; cooling holes were machined by either laser drilling or electrical discharge machining (EDM) as shown in Fig. 14. Deposition of Cr:GAP by EB-PVD proved much more challenging than other ceramic materials. The top of the ingot exploded under e-beam heating and the top of the ingot fractured due to thermal shock (Fig. 15). After many aborted attempts, the top section of the ingot (which may have been too dense) was removed and successful deposition was achieved under extremely gentle electron-beam heating. Specimens with a 25 µm thick Cr:GAP layer were deposited on top of a 200 µm thick TBC. Specimens were shipped to NASA for collecting luminescence emission spectra and decay curves.

After an appropriate heat treatment, luminescence spectra revealed that the desired perovskite structure was achieved, which was a major accomplishment because coatings produced by evaporation can often result in different phases than the source material.

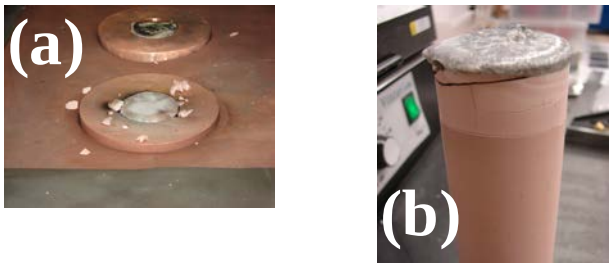

Figure 15. (a) Top of ingot in EB-PVD chamber showing debris from exploding ingot material. (b) Ingot removed from EB-PVD chamber showing fracturing due to thermal shock.

Luminescence decay curves were acquired from the 25-µm-thick EB-PVD Cr:GAP coating with emission intensity even higher than anticipated, resulting in exceptionally high signal-to-noise decay curves from a thin coating, indicating the desired ultra-bright luminescence emission was achieved (Fig. 16). While the decay curves from the coating had a more pronounced fast initial decay than from the puck, fitting to a double exponential gave excellent agreement between the longer decay constants for the puck and coating. Fig. 9 shows that the decay measurements for the coating coincide with the same decay time vs. temperature calibration for the Cr:GAP puck. Based on this excellent outcome, the specimens with cooling holes were shipped to Penn State for Cr:GAP deposition by EB-PVD, and the depositions were performed successfully. Excellent quality luminescence decay curves have been obtained from the specimens with cooling holes. The next step is to attempt 2D temperature mapping of these specimens subjected to a high heat flux produced by laser while cooling air is forced through the cooling holes through the backside of the specimen. This last stage is waiting for a laser repair and the simultaneous availability of the high heat flux laser facility and the time-gated imaging instrumentation, both of which are heavily booked. This final stage of the Phase I effort is scheduled for August-September 2012.

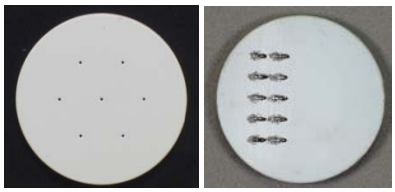

Figure 14. TBC-coated disk with array of 0.020" diameter (left) 90º or 20º (right) cooling holes.

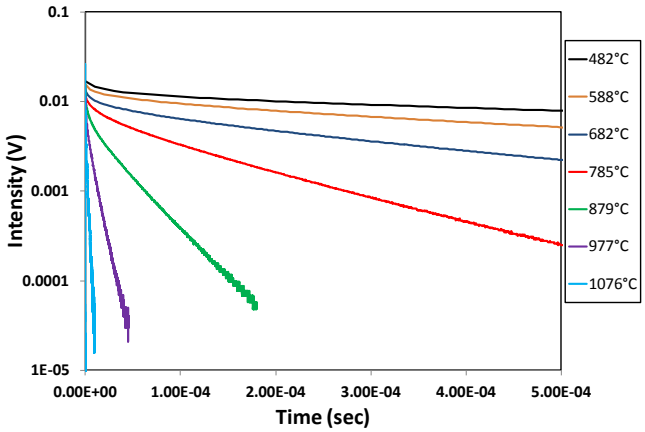

Figure 16. Luminescence decay at various temperatures from EB-PVD Cr:GAP coating. Using bandpass filter centered at 590 nm with a full-width half-max of 40 nm.

Phase I Performance

Phase I Schedule	Date
Produce sapphire fibers with Cr:GAP coated tips.	12/11
In-furnace temperature measurements using sapphire fiber probes	3/12
Establish decay/temperature calibrations	1/12
Develop procedures and optics to optimize time-gated imaging to match the excitation and emission wavelengths and intensities of Cr:GAP luminescence	2/12
Demonstrate surface temperature mapping by time-gated imaging	4/12

The first three scheduled items were completed on schedule (or earlier). Because of the challenges that were eventually overcome in producing the EB-PVD coatings and then the need to simultaneously schedule heavily booked facilities and instrumentation, the final two items are expected to be completed by the end of 9/12.

Phase I Deliverables	Date
1.Working sapphire-fiber-based thermometer with Cr:GAP coated tip demonstrated to 1300°C	6/12
2.Demonstrated 2D temperature mapping around cooling holes in specimen subjected to high heat flux	6/12
3.Draft of paper to be submitted to journal that explains and demonstrates temperature measurements by Cr:GAP broadband luminescence decay	6/12

Status of Deliverables

#1: Working sapphire-rod-based thermometer with Cr:GAP coated tip demonstrated to 1100ºC. Higher purity sapphire fibers or YAG fibers expected to extend performance up to 1200ºC, well above current luminescence-based optical thermometers. These fibers have been procured and delivered and confirmation of their performance is waiting for a laser repair that should be completed in August 2012.

#2: Due to delays explained under Schedule Performance above, 2D temperature mapping around cooling holes is expected to be completed by the end of 9/12, three months later than original delivery date.

#3: Paper titled "Temperature Sensing Above 1000ºC Using Cr-Doped $GdAlO_3$ Spin-Allowed Broadband Luminescence" submitted for Proceedings of the 9th International Temperature Symposium. Follow-up paper on development of Cr:GAP based optical thermometer planned to be submitted in Fall 2012.

Accomplishments

The Phase I Seedling effort demonstrated that a strategic choice of GAP as the matrix material for Cr^{3+} luminescence in combination with utilizing the spin-allowed broadband emission greatly extended the observance of ultra-bright luminescence from the previous state-of-the-art upper limit of 600ºC to 1200ºC, an unprecedented increase in upper temperature capability. A reservoir energy level model was successfully fitted to the temperature dependence of the luminescence decay time and was shown to provide a useful temperature vs. decay time calibration. An optical thermometer composed of a Cr:GAP-coated sapphire lightpipe was demonstrated to 1100ºC. Limitations of temperature performance due to lightpipe impurities were discovered and alternative lightpipes to overcome those limitations have been identified. EB-PVD deposition of Cr:GAP coatings were successfully developed that exhibited remarkably bright luminescence at temperatures above 1000ºC from coatings that were only 25µm thick. TBC-coated specimens with cooling holes were coated with a thin layer of Cr:GAP and are ready for 2D thermal gradient mapping that will be performed in the near future as soon as the testing facilities are available.

Next Steps

The Phase I demonstration of temperature mapping capability will lead to its implementation into NASA test facilities, such as the high heat flux laser facility and high temperature burner rigs, as well as lower temperature application in wind tunnels. The 2D temperature mapping of the area surrounding cooling holes has already attracted interest from the new ARMD Aeronautical Sciences Project as a potential validation tool for the effectiveness of different air film cooling strategies that minimize the temperature variations along the component surface, thereby reducing cooling air requirements and extending component life. In addition, the NASA Vehicle Integrated Propulsion Research (VIPR) project has also expressed interest in using luminescence from Cr:GAP coatings for temperature measurements on turbine blades in an operating F117 engine on a C-17 to monitor blade temperature before and after ingestion of volcanic ash. The ultra-bright luminescence from the Cr:GAP coating is especially attractive for this application because it should still be detected despite attenuation by the overlying volcanic ash deposit. The AFRL VAATE project has expressed interest in both the 2D temperature mapping and on-wing compatible LED excitation as indicated by the offer by AFRL to make available a piggyback engine testing opportunity for testing at AEDC as well as the

probe that was designed by VAATE for engine insertion.

In addition, a proposal for a Phase II Seedling effort has been submitted with the overall goal of demonstrating that temperature measurements using luminescence decay of Cr:GAP that were demonstrated in Phase I can be made in an actual turbine engine environment in a manner that provides key advantages over conventional thermocouple or pyrometer measurements. The two attractive implementations that rely on ultra-bright luminescence demonstrated in phase I that will be developed in phase II for engine demonstration are (1) fast, non-rastered 2D temperature mapping and (2) low-power LED excitation suitable for on-wing diagnostics. Demonstration of 2D temperature mapping for a commercial vane (Fig. 17) in an actual combustion environment will show that these capabilities can be successfully translated into a turbine engine environment. Furthermore, the demonstration of measurements using LED excitation integrated into a probe designed for engine insertion will show that this new approach can be eventually developed for on-wing diagnostics.

Figure 17. Honeywell stator vane doublet selected for 2D temperature mapping around cooling holes in combustion environment for Phase II.

Current TRL: 2

Applicable NASA Programs/Projects

The development of the ultra-bright Cr:GAP thermographic phosphor has attracted considerable interest both within and outside of NASA. This development is expected to be incorporated into the future direction of a task titled "Luminescence-Based TBC/EBC Diagnostics" that will be part of the portfolio of the ARMD Aeronautics Sciences Project (ASP) under the Innovative Measurements Subproject. Discussions on adopting this activity were with Larry Matus, GRC POC for this subproject. As noted in the Next Steps section, interest has also been expressed by the NASA VIPR Project for an important role for the Cr:GAP thermographic phosphor for measuring turbine blade temperatures. These discussions have been with John Lekki, the NASA GRC VIPR POC. Finally, the measurement capabilities of the Cr:GAP thermographic phosphor have attracted significant interest from AFRL for their VAATE Project, which came about through discussions with William Stange (AFRL), and Steve Allison (ORNL). Interest was also expressed by Jim Heidmann, chief of the Turbomachinery and Heat Transfer Branch at GRC, who sought incorporation of the new 2D temperature mapping capability to support validation of new cooling methods as part of a ARMD Phase I Seedling proposal titled "Active Closed-Loop Modulated Turbine Cooling".

Publications and Patent Applications

A patent application was filed in 11/11 titled "Temperature and Pressure Sensors Based on Spin-Allowed Broadband Luminescence of Doped Orthorhombic Perovskite Structures." A presentation was given at the 9th International Temperature Symposium titled "Temperature Sensing Above 1000ºC Using Cr-Doped $GdAlO_3$ Spin-Allowed Broadband Luminescence" in 3/12 and an article with the same title was submitted to the Conference Proceedings. This article has been accepted with only minor revisions requested.